OE Optical Engineering

RESEARCH PAPER

Deep learning assisted far-field multi-beam pointing measurement

Xunzheng Li,[a,b] **Chun Peng**,[c,d,*] **and Xiaoyan Liang**[b,c]

[a]University of Chinese Academy of Sciences, Center of Materials Science and Optoelectronics Engineering, Beijing, China

[b]ShanghaiTech University, School of Physical Science and Technology, Shanghai, China

[c]Chinese Academy of Sciences, Shanghai Institute of Optics and Fine Mechanics, State Key Laboratory of High Field Laser Physics, Shanghai, China

[d]Zhangjiang Laboratory, Shanghai, China

ABSTRACT. We present and experimentally verify a deep learning approach to synchronously measure the multi-beam pointing error for coherent beam combining systems. This approach uses only one detector by acquiring the far-field interference focal spot, which can greatly reduce the complexity in coherent beam combining systems with high accuracy. The amplitude modulation is utilized to eliminate the confusion of the label values in symmetric system. The position assist camera is used to acquire accurate label value, which solves the mismatch between sample and label value caused by ambient vibration in long-term data acquisition. In simulation and experiment, the RMS accuracy is about 0.3 and 0.5 μrad, respectively, which can greatly meet the pointing measurement requirement in coherent beam combining systems. The result shows that this approach can be well applied to multi-beam coherent combination for high-power laser systems.

Keywords: deep learning; multi-beam pointing; measurement; coherent beam combination

Paper 20230142G received Feb. 15, 2023; revised Jun. 25, 2023; accepted Jul. 20, 2023; published Aug. 2, 2023.

1 Introduction

The development of optical parametric chirped-pulse amplification technology promotes the rapid progress of ultra-intense and ultra-short lasers.[1–3] Hitherto, the output of ultra-intense and ultra-short lasers facility have breakthrough 10 petawatts (PW) class.[4–6] Many organizations worldwide are working to further improve the output capacity of ultra-fast lasers.[7] Nevertheless, owing to the damage threshold and the aperture limit, the increase of single-channel output scheme is facing difficult challenges. Coherent beam combination (CBC) is a promising technique to solve the output problem from another direction.[8–10] Experts attempt to combine multi-channel lasers to achieve higher output power. Several institutions have projected to utilize the CBC scheme to improve the output capacity of their ultra-fast laser facilities to the 100 PW class.[5,7]

In CBC research, the beam-pointing (tip and tilt) is a significant parameter that affects the combining efficiency. The pointing synchronization requirement of multi-beam is particularly important when the CBC technique is used in the high-power ultra-fast laser facility. In light of previous research, the beam-pointing error should be controlled below 3.3 μrad to achieve 90% combining efficiency for a multi-channel CBC system with beam aperture of 20 mm.

*Address all correspondence to Chun Peng, pengchun@siom.ac.cn

For 95% combining efficiency, the minimum beam-pointing synchronization requirement of 20 mm beam aperture is 2.4 μrad.[10] It is a tough task to keep the pointing jitter under 5 μrad in such a laser facility. In the common method, the beam-pointing for multi-beam systems is individually monitored by beam position sensors, such as complementary metal-oxide-semiconductor and charge coupled device (CCD). However, the multi-sensor and sampling optics will significantly complicate the experiment structures. Thus, finding a new way to simplify the structure is necessary. For the reason that the pointing of every single beam can affect the focal spot distribution, it is possible to derive pointing errors from the focal spot in multi-beam tiled-aperture CBC systems. Deep learning is believed to be an outstanding solution, due to its excellent image identification performance. In recent years, the application of deep learning in the CBC system has achieved remarkable results, for instance, phase control, wave-front detection, and phase optimization.[11–13] In 2020, our group reported the simulation study of deep learning technology applied to the parameter measurement of CBC system.[14] However, these studies are mostly carried out by theoretical simulation; experimental study is rare. Owing to the influence of experimental factors, practical application in experiment is a great challenge for the deep learning approach. The collection of a large number of samples with accurate label values is crucial in the experiment. Thus, experimental study of deep learning in CBC is of great significance.

Here, we propose a far-field multi-beam pointing measurement approach by using the deep convolutional neural network (DCNN) algorithm for CBC systems. This study is an experimental validation of previous work,[14] which proves the experimental feasibility of using a deep learning method to synchronously measure multi-axis beam-pointing in CBC system. Monitoring the far-field focal spot by only one detector, this approach can greatly simplify the optical structure with high accuracy. We employ the amplitude modulation and the position assist to establish a far-field pattern set which have the one-to-one relationship between each sample and its label value. In this study, we first analyze the theoretical principle to prove in detail the amplitude modulation method can solve the label value confusion problem. Meanwhile, the simulated far-field patterns are utilized to demonstrate the identify capability of DCNN. Then, a two-beam coherent combination setup is built to further verify the practical feasibility of the measurement approach. Furthermore, we also study the influence of ambient vibration on the measurement accuracy.

2 Principle and Simulation

Filled-aperture combining and tiled-aperture combining are two categories of CBC technique. For large aperture ultra-fast lasers systems, tiled-aperture is regarded as a more suitable technique. The beam-pointing instability leads to the separation of far-field focal spot in multi-beam tiled-aperture coherent combination system, which degrades the combining efficiency. In a multi-channel tiled-aperture CBC system, the key task is to increase the peak intensity of the focal spot. Therefore, the combining efficiency of tiled-aperture CBC η_t is usually defined by the peak intensity, which can be written as Eq. (1):

$$\eta_t = \frac{I_{\mathrm{CBC}}}{\left(\sum_n \sqrt{I_n}\right)^2}, \tag{1}$$

where I_n is the peak intensity of the n'th sub-beam, and I_{CBC} is the peak intensity of the combined beam.

We consider a continuous reference laser measurement model involving only beam pointing errors. For n similar Gaussian beams with the same diameter D and wavelength λ, the amplitude, the near-field positions, and the tip/tilt of the n'th sub-beam are A_n, (x_n, y_n), and θ_{xn}, θ_{yn}, respectively. The electric field distribution of the n'th sub-beam is represented as

$$E_n(x,y) = A_n \exp\left[-\frac{(x-x_n)^2+(y-y_n)^2}{\left(\frac{D}{2}\right)^2}\right] \exp\left[i\frac{2\pi}{\lambda}(x\cos\theta_{xn} + y\cos\theta_{yn})\right]. \tag{2}$$

In the far-field, the beam focused by a lens of the focal length f is similar to the Fourier transform

$$E_n(u,v) = \iint E_n(x,y)\exp\left[-i\frac{2\pi(xu+yv)}{\lambda f}\right]\mathrm{d}x\,\mathrm{d}y, \tag{3}$$

where (u,v) is the beam position in the focus plane. So, we can deduce that the far-field distribution of the nth sub-beam as follows:

$$E_n(u,v) = \frac{A_n\pi D^2}{4}\exp\left\{-\left(\frac{\pi D}{2\lambda f}\right)^2[(u-f\cos\theta_{xn})^2+(v-f\cos\theta_{yn})^2]\right\} \times\exp\left\{-i\frac{2\pi[x_n(u-f\cos\theta_{xn})+y_n(v-f\cos\theta_{yn})]}{\lambda f}\right\}. \tag{4}$$

The far-field coherent combination intensity of the n-beam system is

$$I_{\sum}(u,v) = \left|\sum\nolimits_n E_n\right|^2. \tag{5}$$

In this work, we use a Nvidia 2080ti graphic processing unit to simulate and calculate. The numerical simulation of two beams is shown in Fig. 1, where we utilize two beams with a wavelength of 800 nm and a diameter of 6 mm to combine the far-field focal spot in the focal plane with a precision of 4 μm pixels. The far-field interference fringes and near-field beams distribution are shown in Figs. 1(a) and 1(b). We set the beam-pointing vector to $\vec{\theta} = [\theta_{x1},\theta_{y1};\theta_{x2},\theta_{y2}]$, where θ_x is the tip and θ_y is the tilt. According to Eqs. (4) and (5), we can obtain Eqs. (6)–(8):

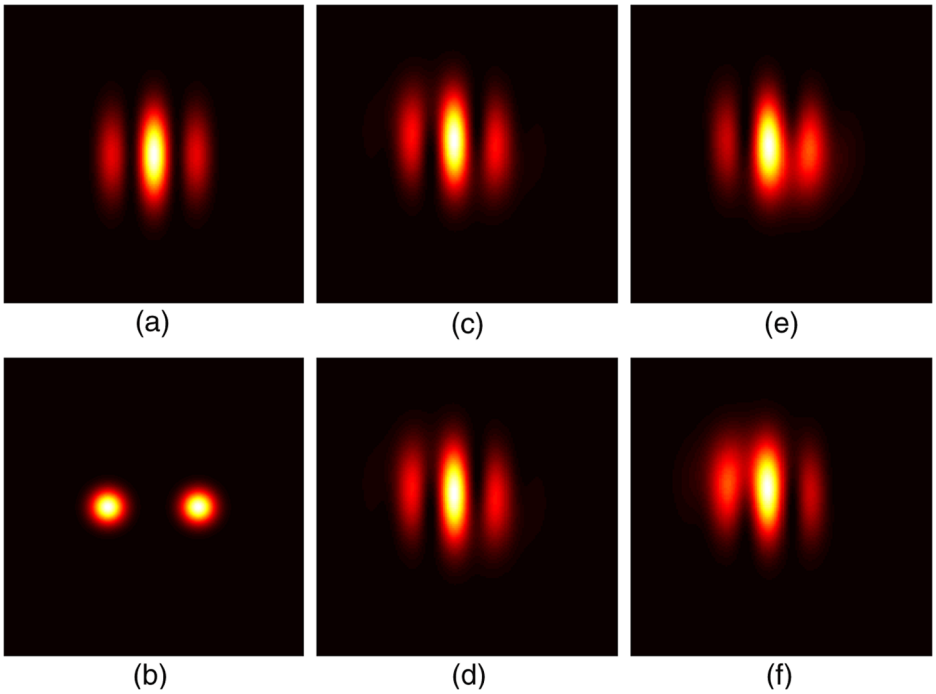

Fig. 1 Simulation of two beams: (a) far-field interference fringes without pointing error, (b) near-field beams distribution, (c), and (d) confusion of label values: far-field interference patterns with the same amplitude, (c) $\vec{\theta} = [20,20;0,0]$ μrad, (d) $\vec{\theta} = [0,0;20,20]$ μrad, (e), (f) far-field interference patterns with amplitude modulation $A_1 = 1$; $A_2 = 1.5$, (e) $\vec{\theta} = [20,20;0,0]$ μrad, and (f) $\vec{\theta} = [0,0;20,20]$ μrad.

$$E_1(u,v)E_2^*(u,v)+E_2(u,v)E_1^*(u,v)=A_1A_2\left(\frac{\pi D^2}{4}\right)^2 \times\exp\left\{-\left(\frac{\pi D}{2\lambda f}\right)[(u-f\cos\theta_{x1})^2+(v-fs\theta_{x2})^2+(u-f\cos\theta_{y1})^2+(v-f\cos\theta_{y2})^2]\right\} \times 2\cos\left\{\frac{2\pi[x_2(u-f\cos\theta_{x2})+y_2(v-f\cos\theta_{y2})-x_1(u-f\cos\theta_{x1})-y_1(v-f\cos\theta_{y1})]}{\lambda f}\right\} \tag{6}$$

$$|E_1(u,v)|^2=\left(\frac{A_1\pi D^2}{4}\right)^2\exp\left\{-2\left(\frac{\pi D}{2\lambda f}\right)^2[(u-f\cos\theta_{x1})^2+(v-f\cos\theta_{y1})^2]\right\}, \tag{7}$$

$$|E_2(u,v)|^2=\left(\frac{A_2\pi D^2}{4}\right)^2\exp\left\{-2\left(\frac{\pi D}{2\lambda f}\right)^2[(u-f\cos\theta_{x2})^2+(v-f\cos\theta_{y2})^2]\right\}, \tag{8}$$

where $E_1(u,v)E_2^*(u,v)+E_2(u,v)E_1^*(u,v)$ is the interference term of beams 1 and 2, $|E_1(u,v)|^2$ and $|E_2(u,v)|^2$ are their intensity term, respectively.

In the deep learning measurement approach, the one-to-one correspondence between the sample and its label value is the premise of achieve excellent measurement result. However, the two beams with symmetrically distributed $(x_1=-x_2;y_1=y_2)$ cannot build this relationship due to the label value confusion, which will lead to the decrease of the recognition effect of DCNN. This phenomenon can be described by Eqs. (6)–(8). When $A_1=A_2$, whether the pointing jitter occurs in beam 1 or beam 2, leads to the same far-field distribution. In this way, the one-to-one correspondence between the far-field pattern and the label value is confused. For example, the far-field interference pattern with the same amplitude is shown in Figs. 1(c) and 1(d), beams 1 or 2 with 20 μrad of tip and tilt present the identical far-field interference fringes. To solve this problem, we employ amplitude modulation for beam 2. So, the $|E_1(u,v)|^2$ and $|E_2(u,v)|^2$ terms in Eqs. (7) and (8) are different. Figures 1(e) and 1(f) show the far-field interference with amplitude modulation. We can see that under amplitude modulation, the beam-pointing change of different beams corresponds to disparate interference pattern. Hence, amplitude modulation is a crucial method to distinguish beams in symmetric multi-beam systems.

To achieve high precision measurement, proper network construction is essential. In this work, we modify part of the layers of a mature Google inception-v3 model for transfer learning to save calculation time.[15,16] For the input layers, the input data are replaced by the pseudo color far-field interference patterns of size $160\times160\times3$ and its label values to meet the network standard. The last layer is substituted for the beam-pointing vector and retrained. In this way, the output data are the beam-pointing error value identified by DCNN. Furthermore, we employ the mean squared error (MSE) as the loss function of the DCNN model. The loss function is expressed as $L(\mathrm{MSE})=\|\vec{\theta}_{np}-\vec{\theta}_{nl}\|^2$ and, where $\vec{\theta}_{np}$ and $\vec{\theta}_{nl}$ are the beam-pointing vector predicted by the DCNN and the corresponding label vector of the n'th sample.

Figure 2 shows the training process of DCNN. We feed the far-field pattern samples with label values into the DCNN pre-scheme. The network calculates the loss function base on $\vec{\theta}_{np}$ and $\vec{\theta}_{nl}$ to adjust its weight. Through multiple iterations of training, the loss function is optimized to the expected value. To test the performance of the trained DCNN model, some untrained samples of testing set are fed into the DCNN model for measurement. The result of the testing set can reflect the generalization of DCNN, which is the ability of the DCNN model to recognize new data.

We randomly generate 21,000 far-field interference pattern samples with different label values, the tip and tilt of each beam is within $[-20,20]$ μrad. The other simulation parameters of the training samples are identical to Fig. 1. We use 14,000 samples as the training set, 6000 samples as the validation set, and the other 1000 samples as the testing set. Here, we define the deviation of the beam-pointing error is the absolute value of the predicted value subtracted from its label value. The simulate root mean square (RMS) value of the beam-pointing deviations is $[0.203, 0.272, 0.171, 0.180]$ μrad. To evaluate the performance of DCNN, the maximum beam-pointing deviations 0.2722 μrad is adopted. It shows that the theoretical RMS accuracy of

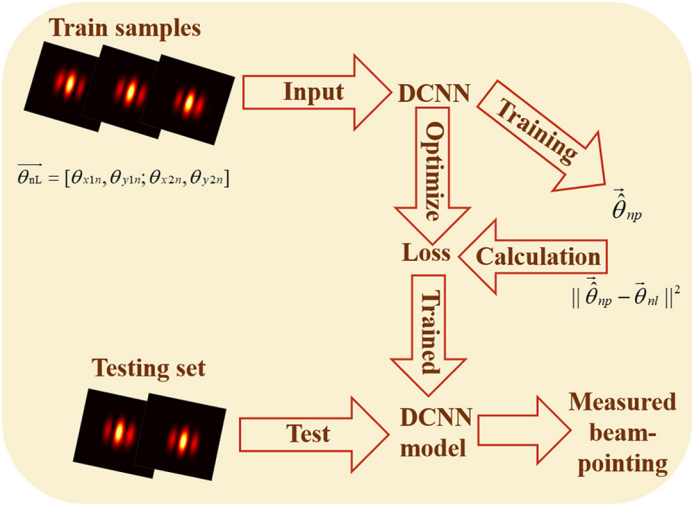

Fig. 2 Training and measurement process of DCNN.

this approach is <0.3 μrad, which completely accord with the pointing synchronous requirement of high combining efficiency tiled-aperture CBC system.

3 Experiment

The simulation result theoretically demonstrates the feasibility and the accuracy of the far-field beam-pointing measurement approach. In this section, we carry out two-beam pointing measurement experiment to further evaluate the practical performance of this approach. As shown in Fig. 3, a two-beam coherent combination sample acquisition setup is constructed. A 50% beam splitter divides a continuous-wave laser with a wavelength of 808 nm into two beams. A half wave plate is used to modulate the amplitude ratio of beams 1 and 2. In this experiment, the amplitude intensity of beam 2 is modulated to 1.5 times that of beam 1. The beam diameter is extended to 6 mm by the beam expander. Two piezoelectric inertia actuators are used to adjust the tip and tilt of beams 1 and 2. The far-field interference fringe pattern is generated by focusing beams 1 and 2 into the same lens with a focal length of 750 mm. Here, we use a CCD camera 1 with 4 μm pixel resolution to collect the pattern as the training sample for DCNN. To avoid the mismatch between the sample and label value caused by ambient vibration, we use cameras 2 and 3 monitoring the far-field position of two beams as the position assist camera to obtain precise

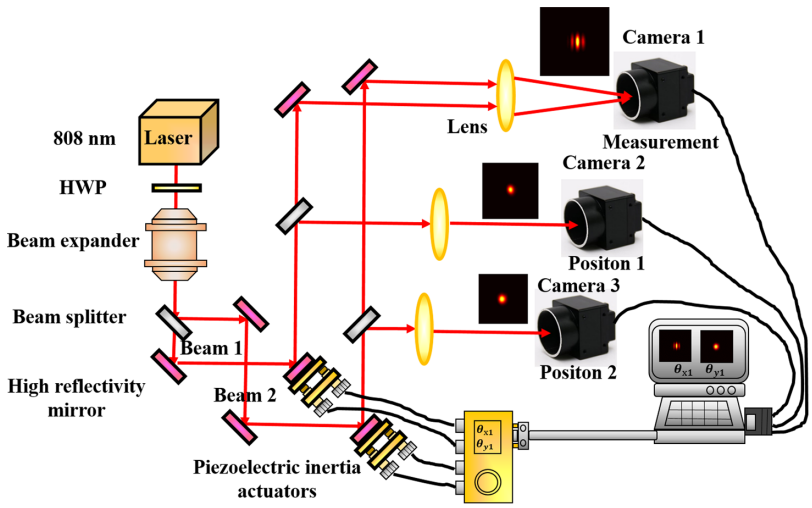

Fig. 3 Sample acquisition setup. Here, cameras 2 and 3 are only employed for label value assistance in the sample collection stage. These two cameras are designed to reduce the influence of non-experimental factors. In the measurement stage, only camera 1 is used.

label values of the training sample. The focal length of the lens before camera is 600 mm. We regard the center of mass of the focal spot as the center of the monitored beam, so we can calculate the beam-pointing change based on the movement of the center of mass of the focal spot. Center of mass algorithm can be used to calculate the change of beam-pointing of 1/100 pixels. Compared with directly recording the change of piezoelectric inertia actuator, center of mass algorithm can obtain more accurate label values. Note that during the measurement stage, only camera 1 is used.

First, we control the piezoelectric inertia actuator to collect 11,000 far-field interference pattern samples with different pointing label values under low ambient vibration conditions. These experimental samples are utilized to train the DCNN model, and the train process is the same as in part 2. We use these samples as the training set, the validation set and the testing set in a ratio of 7:3:1. Figure 4 shows the experimental data and results. The experimental far-field pattern and the loss function curve during training are shown in Figs. 4(a) and 4(b). The training curve illustrates that the loss function of the training and validation set convergent rapidly with the epoch increase. This also shows that the model has stable and excellent performance. Figures 4(c) and 4(d) show the tip and tilt deviation distribution of beams 1 and 2 for 1000 testing samples. The RMS values of the testing set on the trained DCNN model is $[0.384, 0.452; 0.372, 0.489]$ μrad. In general, the experimental results show good agreement between theory and experiment on performance of DCNN for the reason that the pointing synchronization requirement for 95% combining efficiency of the CBC system with 6 mm beam aperture is about 8 μrad; 0.5 μrad is quite excellent accuracy.

However, due to the inaccurate label value, there is a certain deviation between the experimental results and the theoretical results. Ambient vibration is the main factor that affect DCNN performance in experiment. The actual pointing instability of the far-field interference pattern may be slightly different from its label value under the vibration disturbance of the surrounding instrument. To clarify the influence of ambient vibration on the measurement performance of DCNN, we carry out further study.

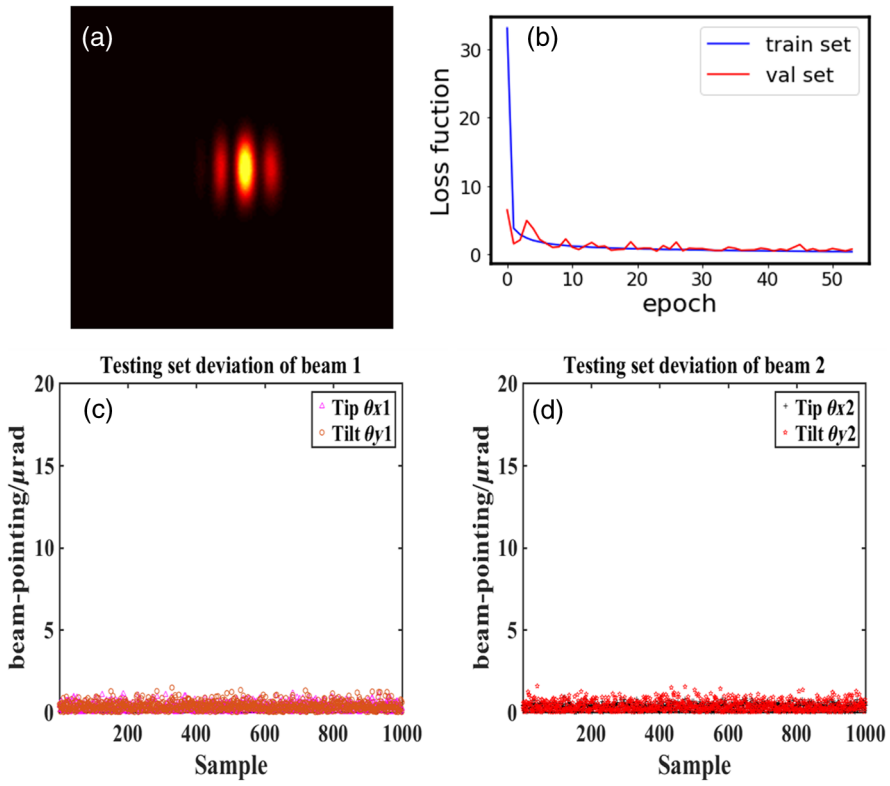

Fig. 4 Experimental data and results. (a) Far-field interference fringes patterns without pointing error. (b) MSE changes of training and validation set during training. (c), (d) The tip and tilt test deviation of 1000 testing set samples. (c) Beam 1 and (d) beam 2.

Then, we collect 11,000 patterns in high ambient vibration to consider the effect of ambient vibration on measurement capacity. The proportion of training, validation, and testing set are the same as before. The RMS value of beam-pointing in high ambient vibration is $[1.336, 1.210; 1.213, 1.115]$ μrad. There are significant differences between the measurement results of the two ambient vibration. This phenomenon indicates that the high ambient vibration has a great influence on our method. Hence, a vibration isolation environment would increase the measurement accuracy of DCNN.

Finally, to comprehensively consider the measurement capacity, 16,000 far-field interference patterns are randomly selected from the two ambient vibrations, of which 10,500 are utilized as the training set, 4500 as the validation set, and other 1000 samples as testing set. We can obtain the RMS accuracy of testing set is $[0.694, 0.665; 0.603, 0.685]$ μrad. The results are between two ambient vibrations, which supports the conclusion that low ambient vibration can improve the measurement accuracy of DCNN.

In this section, we apply the DCNN method to the two-beam coherent combination setup, which achieved excellent performance. The measurement results in different environments show that reducing ambient vibration can obtain more accurate measurement results. On the basis of experimental results, this approach is feasible to simplify the optical structure and has high measurement accuracy. In the future, we will attempt to apply the deep learning technology to the measurement and control of more complex multi-beam coherent combination systems.

4 Conclusion

In summary, a deep learning assisted far-field multi-beam pointing measurement approach is presented. This approach employs the far-field interference pattern to train the DCNN model to recognize the multi-beam pointing error simultaneously. The amplitude modulation method is introduced to distinguish the beam-pointing variation in symmetric CBC systems. We initially employed the simulated two-beam far-field interference as training samples to verify the feasibility and accuracy. The RMS value was <0.3 μrad. Afterward, we build a two-beam coherent combination experimental setup to verify the generalization ability of DCNN model. The measured RMS value of beam-pointing error achieves 0.5 μrad in the experiment. The influence of ambient vibration is studied. The RMS value of high ambient vibration and comprehensive ambient vibration are about 1.3 and 0.7 μrad, respectively. The measurement results show that the approach has high precision performance and well meets the pointing synchronous requirement of 95% combining efficiency of CBC system. It is of great significance for simplifying the measurement optical structure of a multi-beam coherent combination system.

Code, Data, and Materials Availability

The data in this manuscript are publicly available in scienceDB at https://doi.org/10.57760/sciencedb.08484.

Acknowledgments

This work was supported by the Shanghai Science and Technology Innovation Action Plan Project (Grant No. 19142202500), National Natural Science Foundation of China (NSFC) (Grant No. 11974367), and the Program of Shanghai Academic/Technology Research Leader (20SR014501). The authors declare that they have no known competing financial interests or personal relationships that may have influenced the work reported in this study.

References

1. D. Strickland and G. Mourou, "Compression of amplified chirped optical pulses," *Opt. Commun.* **55**(6), 447–449 (1985).
2. A. Dubietis, G. Jonušauskas, and A. Piskarskas, "Powerful femtosecond pulse generation by chirped and stretched pulse parametric amplification in BBO crystal," *Opt. Commun.* **88**(4-6), 437–440 (1992).
3. J. Bromage et al., "MTW-OPAL: a technology development platform for ultra-intense optical parametric chirped-pulse amplification systems," *High Power Laser Sci. Eng.* **9**(4), 04000e63 (2021).

4. W. Li et al., "339 J high-energy Ti:sapphire chirped-pulse amplifier for 10 PW laser facility," *Opt. Lett.* **43**, 5681–5684 (2018).
5. Z. Gan et al., "The Shanghai superintense ultrafast laser facility (SULF) project," in *Progress in Ultrafast Intense Laser Science XVI*, K. Yamanouch, K. Midorikawa, and L. Roso, Eds., p. 199, Springer International Publishing, Cham (2021).
6. C. Radier et al., "10 PW peak power femtosecond laser pulses at ELI-NP," *High Power Laser Sci. Eng.* **10**, e21 (2022).
7. C. N. Danson et al., "Petawatt and exawatt class lasers worldwide," *High Power Laser Sci. Eng.* **7**, e54 (2019).
8. C. Peng et al., "Two-beam coherent combining based on Ti:sapphire chirped-pulse amplification at the repetition of 1 Hz," *Opt. Lett.* **44**, 4379–4382 (2019).
9. C. Peng et al., "Four-beam tiled-aperture coherent beam combining of high-power femtosecond laser with two compressors," *IEEE Photonics J.* **14**, 3305804 (2022).
10. S. N. Bagayev et al., "Super-intense femtosecond multichannel laser system with coherent beam combining," *Laser Phys.* **24**, 074016 (2014).
11. T. Hou et al., "Deep-learning-based phase control method for tiled aperture coherent beam combining systems," *High Power Laser Sci. Eng.* **7**(4), 04000e59 (2019).
12. L. Hu et al., "Deep learning assisted Shack–Hartmann wavefront sensor for direct wavefront detection," *Opt. Lett.* **45**, 3741–3744 (2020).
13. B. Mills et al., "Single step phase optimisation for coherent beam combination using deep learning," *Sci. Rep.* **12**, 5188 (2022).
14. R. Liu et al., "Coherent beam combination far-field measuring method based on amplitude modulation and deep learning," *Chin. Opt. Lett.* **18**, 041402 (2020).
15. C. Szegedy et al., "Rethinking the inception architecture for computer vision," in *IEEE Conf. Comput. Vision and Pattern Recognit. (CVPR)*, pp. 2818–2826 (2016).
16. S. J. Pan et al., "Domain adaptation via transfer component analysis," *IEEE Trans. Neural Networks*, **22**(2), 199–210 (2011).

Xunzheng Li received his BEng degree from the School of Nankai University, Tianjin City, China. Currently, he is a doctor's degree candidate at Shanghaitech University, Shanghai City, China. He is mainly engaged in the research of ultra-intense and ultra-short lasers.

Chun Peng received her doctor's degree from the Shanghai Institute of Optics and Fine Mechanics, Shanghai City, China. Currently, she is an associate researcher at Zhangjiang Laboratory, Shanghai City, China. She is mainly engaged in the research of laser technology and coherent beam combining.

Xiaoyan Liang received her doctor's degree from the Institute of Physics CAS, Beijing City, China. Currently, she is a researcher at Shanghai Institute of Optics and Fine Mechanics, Shanghai City, China. She is mainly engaged in the research of laser technology and nonlinear optics.